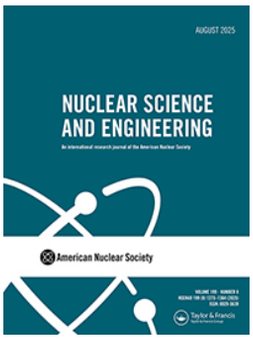

Nuclear Science and Engineering

ISSN: 0029-5639 (Print) 1943-748X (Online) Journal homepage: www.tandfonline.com/journals/unse20

Introduction, Investigation, and Experimental Validation of a Novel Passive Neutron Spectrometer

Zachary T. Condon, Daniel Siefman, Paul Maggi, Paige Witter & Richard Vasques

To cite this article: Zachary T. Condon, Daniel Siefman, Paul Maggi, Paige Witter & Richard Vasques (13 May 2025): Introduction, Investigation, and Experimental Validation of a Novel Passive Neutron Spectrometer, Nuclear Science and Engineering, DOI: 10.1080/00295639.2025.2458437

To link to this article: https://doi.org/10.1080/00295639.2025.2458437

Published online: 13 May 2025.

NUCLEAR SCIENCE AND ENGINEERING
DOI: https://doi.org/10.1080/00295639.2025.2458437

Introduction, Investigation, and Experimental Validation of a Novel Passive Neutron Spectrometer

Zachary T. Condon,[a]* Daniel Siefman,[b,c] Paul Maggi,[b] Paige Witter,[b] and Richard Vasques[a]

[a]*The Ohio State University, Department of Mechanical and Aerospace Engineering, 201 West 19th Avenue, Columbus, Ohio 43210*
[b]*Lawrence Livermore National Laboratory, Nuclear Criticality Safety Division, 7000 East Avenue, Livermore, California 94550*
[c]*University of California, Berkeley, Department of Nuclear Engineering, 2505 hearst Avenue, Berkeley, California 94709*

Received July 5, 2024
Accepted for Publication January 10, 2025

Abstract — *Unfolding neutron energy spectra are instrumental for determining personal health effects and calculating dose received. This area of study is heavily researched, and Lawrence Livermore National Laboratory (LLNL) is investigating a passive neutron spectrometer for the purpose of acquiring the information needed to determine personnel dose in the event of a criticality accident. A part of this investigation is presented in this article through the examination of four experimental detector responses (DRs). These four DRs were acquired in the presence of ^{252}Cf, AmBe, GODIVA, and National Ignition Facility (NIF) neutron sources. An algorithm developed at LLNL was used to unfold the neutron fluence from each of the four DRs, and subsequently, fluence-to-dose conversion factors provided by the American National Standards Institute were used to calculate dose. Additionally, a multistep unfolding process was developed and employed to calculate the effects of both direct (from the source) and indirect (from room return) neutrons. The average error when unfolding the direct DR was less than 8%. The dose from ^{252}Cf was predicted with only 8% error. The multistep approach allowed for the identification of the low-energy neutrons in the ^{252}Cf, AmBe, and NIF DRs.*

Keywords — Passive neutron spectrometer, neutron spectrum unfolding.

Note — *Some figures may be in color only in the electronic version.*

I. INTRODUCTION

The ability to unfold neutron spectra is a complex yet necessary challenge that is crucial for determining radiation dose. National and international government organizations set standards on how accurately this dose must be measured and calculated.[1] On a regular basis, the capabilities of nuclear enterprises around the world are tested through international exercises and must achieve within 30% error for neutron dose measurements.[1,2] To acquire dose information, an accurate representation of the neutron energies, or spectrum, is required to be used with energy-dependent radiation dose weighting factors.[3–5]

*E-mail: zachary.condon.6@us.af.mil

In the case of other forms of radiation, like gamma rays, the energy incident on the detector can be resolved within the detector itself. Unfortunately, determining the energy of neutrons incident on a detector is not so easy.[6] Neutrons, being uncharged particles, cannot be directly manipulated into interacting with a detector like charged particles can be. Additionally, the transfer of energy during a neutron interaction is stochastic and can sometimes be overshadowed by excess energy emitted by a nucleus following the interaction. As such, any information detected by a neutron interacting with a detector medium cannot be directly attributed to the initial energy of that neutron.[7]

Typically, a neutron detector is composed of a material with a high interaction cross section for thermal neutrons, such as ^{3}He or ^{6}Li. To detect fast neutrons, the detector is engineered to measure the effects of elastic scattering on protons.[8] None of these materials provide the capability to determine the energy of an incident neutron. However, there have been efforts to develop detection systems that can discriminate between fast neutrons, thermal neutrons, and gamma rays through the combination of scintillation materials and ^{6}Li.[9,10]

The detectors employed in this research were thermoluminescent dosimeters (TLDs) comprising ^{6}L. This isotope of lithium has a cross section of interaction with neutrons that is inversely dependent on the incident neutron energy. Although a single detector cannot determine the energy of incident neutrons, research has shown that arrays of detectors within varying amounts of moderating material, along with an appropriate algorithm, can unfold the energy of incident neutrons. In the last several decades, numerous detection systems and unfolding methods have been developed and employed for this purpose.[11–19]

Lawrence Livermore National Laboratory (LLNL) and The Ohio State University are working on a neutron detection system called the passive neutron spectrometer (PNS) to measure neutron spectra and estimate neutron doses. This paper introduces the PNS system, the modeling used to support it, and measurements to validate its performance. The PNS consists of a ball of high-density polyethylene with neutron detectors placed inside at various depths. It supports both gold activation foils and TLDs as neutron detectors. For multidetector systems, such as the PNS, the set of detector responses (DRs) and the corresponding neutron spectrum can be represented as a linear system of equations related by the detector response matrix (DRM).[13] This requires the discretization of the continuous neutron energy spectrum into specific energy bins.[13] The system can be written as Eq. (1), where the discretized spectrum S is a $[1 \times m]$ vector, where m is the number of energy groups, and the measured DR is a $[1 \times n]$ vector, where n is the number of DRs:

$$S_{[1\times m]}R_{[m\times n]} = \mathrm{DR}_{[1\times n]} \ . \tag{1}$$

Equation (1) introduces the final term R, an $[m \times n]$ matrix, which is the DRM and is described in Sec. III. Mathematically, this equation can be solved for S, which would require psuedo-inverting the DRM. Unfortunately, the solution of the resulting linear equations is nonunique and cannot be used directly to determine the energy spectrum of neutrons. Algorithms, such as MAXED, have been developed for the purpose of unfolding neutron spectra but require an input a priori spectrum as well as a well-characterized DRM.

To obtain the DRM, MCNP simulations of the PNS were conducted. A number of simulation strategies were investigated and analyzed to optimize the performance of the DRM in reference neutron spectra. Algorithms, such as MAXED, require an input a priori spectrum and heavily rely on the accuracy of that input.[13] For well-characterized sources, such as ^{252}Cf and AmBe, an accurate a priori spectrum can be obtained from literature, but in an unknown neutron field, the accuracy of results cannot be easily determined. This led to the development of an in-house iterative algorithm, by Maggi, which will be reported in a companion paper.

The inspiration for Maggi's algorithm came from the purpose of the PNS. It is planned to be used to monitor a criticality accident, which would have an unknown neutron field. Additionally, four experimental DRs for the PNS were obtained, each separately in the presence of ^{252}Cf, AmBe, a GODVIA reactor, and at the National Ignition Facility (NIF). Each of these DRs is unfolded, and for ^{252}Cf and AmBe, the spectrum is compared to reference spectra provided by the International Atomic Energy Agency (IAEA).[3] Several experiments have been conducted to determine the spectrum emitted by the GODIVA reactor, the results of which are compared to the results obtained in this research. The spectrum at the location of the PNS when detecting neutrons at the NIF facility is not characterized.

II. PASSIVE NEUTRON SPECTROMETER

In neutron spectroscopy, a variety of techniques are available, each with associated benefits and drawbacks.

For example, a common approach is the multiple-sphere system, or Bonner spheres, which consists of thermal neutron detectors surrounded by variously sized moderating spheres.[11] Although moderating the neutrons causes a loss of information, varying the moderating sphere size causes each detector to observe a uniquely modified neutron spectrum that depends on the field's neutron spectrum and the thickness of the moderator. This energy dependence can be used to extract the neutron spectrum from a series of detections by the whole system. A drawback is that it needs multiple recordings and requires an operator and a high-voltage power supply.

Previous work designed a passive multidetector neutron spectrometer that requires only one measurement.[20] A similar detection system, the PNS, was manufactured by LLNL to measure neutron spectra and thereby derive dose in the event of a criticality accident. The PNS incorporates 55 detectors, either TLDs or gold activation foils, in a 30-cm-diameter high-density polyethylene sphere as seen in Fig. 1. The detectors are placed along the three Cartesian axes. The TLDs are a combination of TLD-600, which is a neutron-sensitive LiF detector enriched in ^{6}Li, and TLD-700, which is a neutron-insensitive LiF detector enriched in ^{7}Li. In this study, the response of only TLD-600 was used. Future work will include the effects of ^{7}Li, which may provide more accurate results.

In all six directions ($\pm X$, $\pm Y$, $\pm Z$), the detectors are at the following distances from the center: 3, 6, 8, 9, 10, 11, 12, 13, and 14 cm. One final detector is placed at the center, orthogonal to the X-axis. For this initial implementation of the PNS, the placement of sources was not optimized. Rather, the placements follow a similar pattern to the sizing of Bonner spheres. The arrangement allows for exploration of the unique information that can be obtained with detectors spaced in three dimensions. For example, this research used a subset of the detectors to unfold the high-energy part of the spectrum and the remaining detectors to unfold the low-energy part of the spectrum. This process is described more fully in Sec. V.

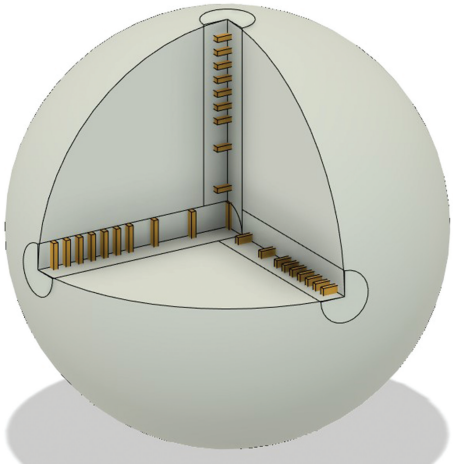

Fig. 1. Model of the PNS.

The major benefits of the PNS are that the detectors are all contained within one sphere, so only a single measurement in the neutron field is required, and because both TLDs and gold foils do not require power, the system will make all measurements passively. This fits well with the intended purpose of providing the information needed to determine the neutron spectrum in an accident scenario. The PNS can be set in place and be read if an accident occurs. Its low-cost design means it can also be placed in multiple locations. The use of TLDs or gold foils depends on the application case: TLDs will need to be periodically replaced but can provide continual monitoring of the neutron environment. The decay of gold activation means that no active interaction with the PNS is necessary, except in the event of an accident. The PNS will need to be collected, and the gold foils will need to be read in a prompt manner; otherwise, information about the accident will be lost within the 2.7-day half-life of ^{198}Au. This may not be possible during an evolving and unknown criticality accident scenario. Although either detector can be used, the experimental DRs unfolded in this work were obtained using TLDs.

In this work, two steps must be performed to determine personnel dose in the presence of neutrons. First, the neutron spectrum, after being unfolded, is multiplied by the fluence-to-dose conversion factors. To ensure that the energy bin structure matches, the conversion factors as reported by the American National Standards Institute (ANSI) are linearly interpolated to the 84 energy groups that will be described in Sec. III.[5] This multiplication results in a single value in units of picosievert but is not yet the true dose. This is because in the unfolding algorithm, the spectrum is normalized such that it sums to one and the calculated dose corresponds to the dose received per neutron. To determine the true dose given an experimental PNS DR, the neutron spectrum must be folded into the DR function (described in Sec. III), and the ratio of the experimental DR to the calculated DR will scale the normalized dose to be the unnormalized dose.

III. DETECTOR RESPONSE MATRIX

The information recorded by the PNS in a neutron field is the DR. It consists of 55 values, each corresponding to one of the TLDs. Furthermore, each detector's

response corresponds to the integral effect of interactions from neutrons at all energies. The spectrum unfolding algorithm, described in Sec. V, requires the use of a DRM, which contains the information for how each detector responds to monoenergetic neutrons. In other words, the DRM is the mathematical representation of the PNS and maps an input neutron spectrum to the associated DR. For the PNS, the full DRM is a matrix of size 55 × 84, where 55 corresponds to the number of detectors and 84 corresponds to the number of energy bins ranging from 1E-3 eV to 100 MeV.

III.A. Simulated DRM

To obtain a DR function, a model of the PNS and a monoenergetic neutron source was made. The monoenergetic neutron source creates a response in each of the 55 detectors specific to that neutron energy. The Monte Carlo N-Particle (MCNP6.2) code was chosen to conduct these simulations.[21] The PNS was modeled as a 30-cm polyethylene sphere with positioning tubes, modeled as right circular cylinders along the three Cartesian axes. Along the length of each positioning tube, slots containing TLD-600s and TLD-700s were modeled. Each TLD was modeled as a rectangular parallelepiped with a Kapton casing surrounding the TLD material. The location on each Cartesian dimension corresponded to measured values in the as-constructed PNS, and any remaining space in the simulation was filled with moist air. Thermal neutron scattering with the $S(\alpha, \beta)$ treatment for hydrogen in polyethylene was used in the simulations. All cross sections used in the simulations were taken from the nuclear data library ENDF/B-VIII.0.[22] Neutrons, alpha particles, protons, and electrons were transported and tallied in the TLDs with +F6 cards. As a variance reduction technique, the cells containing the TLD material were given higher neutron importance.

III.B. Simulated Neutron Sources

One of the primary purposes of the PNS is to obtain a DR in the event of a criticality accident.[23] For this work, we assumed the PNS would be placed in the facility such that a principal Cartesian axis was aligned with the fissile material operation where the accident occurred. Therefore, the first simulated source of neutrons was a planar source on the X-axis at 25 cm from the center of the PNS. Neutrons were directed from this source in the negative X direction and parallel to the X-axis. Each simulation consisted of monoenergetic neutrons, resulting in 84 total simulations for the full DRM.

The MCNP simulation of the PNS did not include anything beyond the PNS itself and the aluminum stand used to hold it. As such, there was nothing that could cause backscatter, which would occur in a real-world scenario. Because of this, a second neutron source was simulated to capture the behavior of the PNS in the presence of backscatter neutrons at all energies. This second source was a 50-cm sphere, centered on the PNS, in which the neutrons were directed inward. Again, each simulation used monoenergetic neutrons, and in total, 84 simulations were performed to create the second DRM specific to backscattered neutrons.

To record the interactions of neutrons in the TLD material, a +F6 tally was used. To capture all of the interactions of secondary particles, physics were enabled for neutrons, photons, electrons, and protons. To increase the accuracy of each tally, the cell for each tally was given an importance of three for all particles. The number of particles was set to 1e10 for each simulation.

Figure 2 shows all of the DR functions for the planar source and spherical source simulations along the three axes. Note that the +F6 tally records the total energy deposition per starting particle and that in each of the graphs, the DR is in units of mega-electron-volts per gram per starting particle. In each figure, the response functions are shaded from dark to light, where the darkest line corresponds to the detector farthest along the respective positive axis and the lightest line corresponds to the detector farthest along the respective negative axis. Figure 2a most clearly shows the progression of response functions from positive (closest to the neutron source) to negative (farthest from the neutron source). The other figures have shaded lines that are almost directly overlapping because the response functions are symmetrical about the center of the detector. For example, the detector at $Y = +14$ cm has the same response function as the detector at $Y = -14$ cm. Also of note is that the Y-axis and Z-axis planar source DRMs (Figs. 2c and 2e) are similar. The nature of the plane source of neutrons causes each set of detectors to respond in the same way. Similarly for the spherical source DRM, the neutrons are coming into the detector from all directions, and the response functions show the six-way symmetry of the PNS.

III.C. Unit Conversion

The output of the +F6 tally in MCNP is in units of mega-electron-volts per gram per source particle and

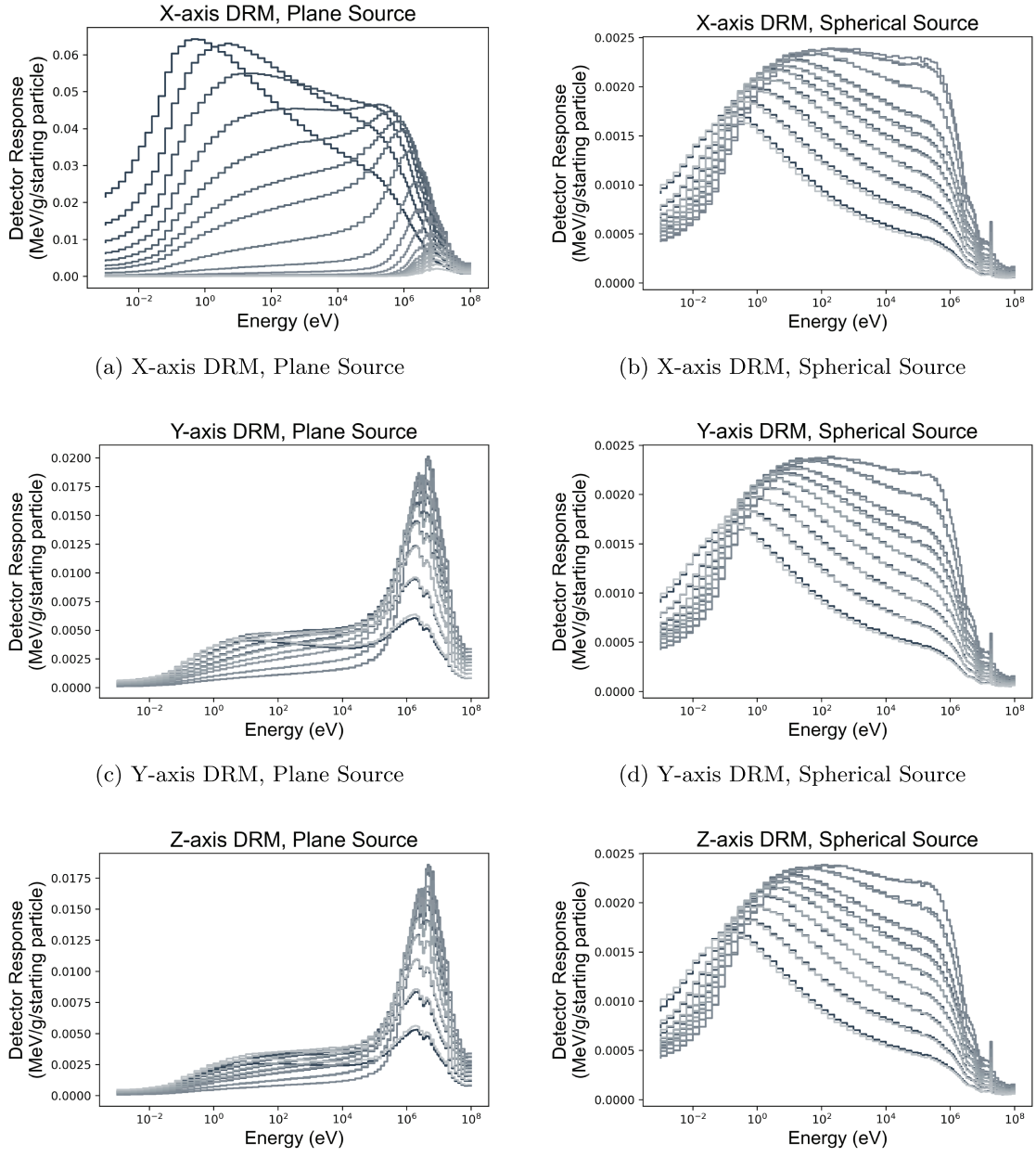

(a) X-axis DRM, Plane Source

(b) X-axis DRM, Spherical Source

(c) Y-axis DRM, Plane Source

(d) Y-axis DRM, Spherical Source

(e) Z-axis DRM, Plane Source

(f) Z-axis DRM, Spherical Source

Fig. 2. The two DRMs used in this research, separated by axis. Detector placement is noted by the shading. The detector closest to the surface on the positive axis is darkest, and the opposite detector is lightest.

needs to be converted to the equivalent operational output of the TLDs (in units of milliroentgens). In this research, the output of the TLDs is calibrated to the equivalent dose absorbed by 662-keV photons from ^{137}Cs. The first step is to convert from units of mega-electron-volts per gram per source particle to units of absorbed dose in LiF per unit neutron fluence (grays per centimeters squared). This is achieved through the following relationship:

$$D_{i,j} = F_{i,j} \times q_e \times M \times A_S \quad , \tag{2}$$

where $F_{i,j}$ = tally result at energy i for detector j; $q_e = 1.602 \times 10^{-13}$ J/MeV; $M = 1000$ g/kg; $A_s = 1509.12$ cm^2, which is the area of the planar source.

To obtain the factor to convert from absorbed dose to equivalent dose, TLD-600 was modeled as described above but within a modeled cylindrical polymethyl methacrylate (PMMA) rod phantom with a 2-cm buildup layer between

the TLD and the source. A simulated 662-keV expanded beam of photons was directed at the rod, and the interactions with the TLD were recorded with the +F6 tally. The total energy deposition of 2.54×10^{-3} MeV/g per source particle was converted to absorbed dose in LiF per unit fluence (1.1×10^{-12} Gy·cm^2). Using Table A.1 of ICRP Publication 116,[24] the antero-posterior effective dose per unit fluence for 662-keV gammas is 3.17 pSv·cm^2. The factor to convert from the absorbed dose in LiF to effective dose is calculated by dividing the effective dose by the absorbed dose:

$$R = \frac{D_e}{D_a} \quad , \tag{3}$$

and the conversion factor is 2.881×10^3 mSv/Gy.

IV. EXPERIMENTAL DRS

To obtain real-world DRs, the PNS was placed in the presence of four neutron sources: ^{252}Cf, AmBe, GODIVA, and NIF. In each experiment, the PNS was equipped with TLDs. The DRs from each neutron source are given in Fig. 3, with units of millisieverts according to the conversion scheme outlined in Sec. III.C. To simplify the presentation of data, all 55 responses are graphed on a two-dimensional plot. The *X*-axis responses are represented as detectors numbered 1 to 19, the *Y*-axis responses are numbered 20 to 37, and the *Z*-axis responses are numbered 38 to 55. A few features stand out in each figure. Namely, the positive *X*-axis detectors have the highest response, and the negative *X*-axis detectors have the lowest response. The *Y*-axis and *Z*-axis detectors show the symmetry of the detector when subjected to a neutron source that is on the *X*-axis.

In all but Fig. 3d, a simulated DR is also shown. This simulated response was obtained by using the same MCNP input deck that was used for the DRM, with the exception of the source card. In place of a monoenergetic neutron source, a histogram source was used with probabilities associated with each neutron source in Figs. 3a, 3b, and 3c. The

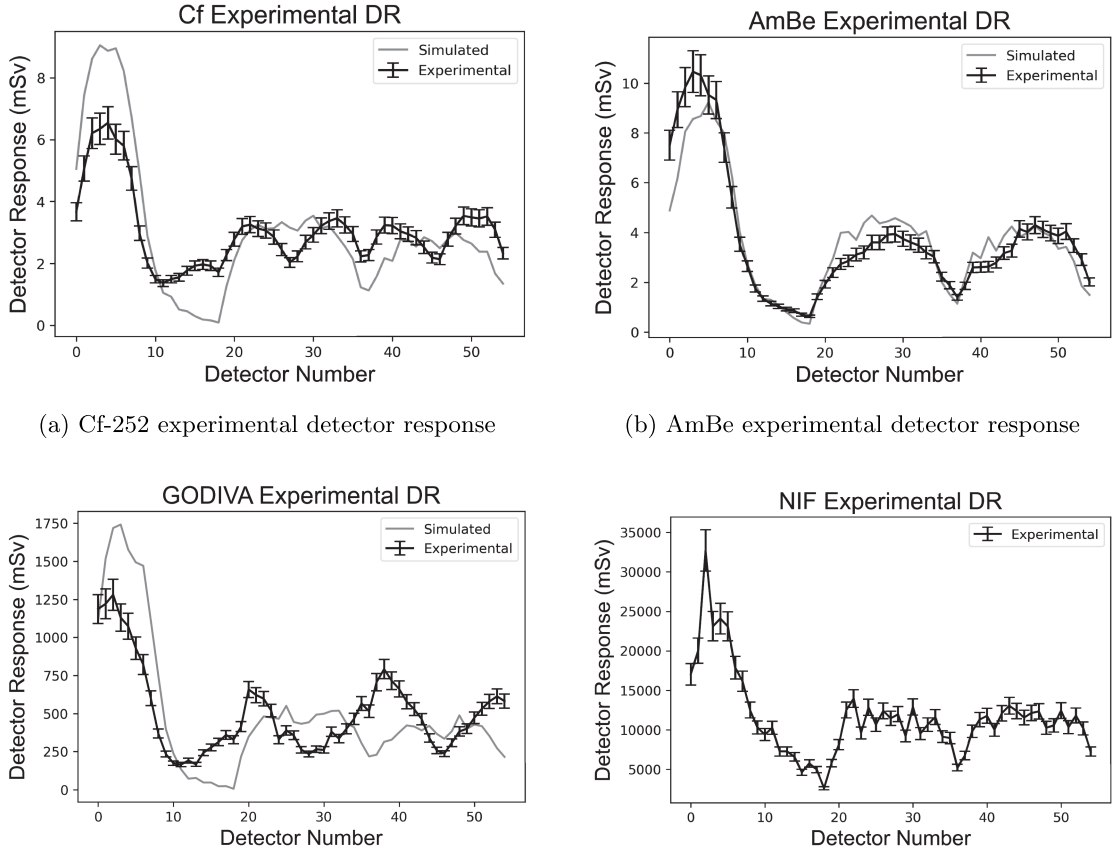

(a) Cf-252 experimental detector response

(b) AmBe experimental detector response

(c) GODIVA experimental detector response

(d) NIF experimental detector response

Fig. 3. The experimental DRs from the PNS in four separate experiments. The error bars in each graph are 8% of the detector value at each point. This value was determined experimentally for the TLDs used in the PNS.

simulated spectrum used for the ^{252}Cf and AmBe was obtained from the IAEA Compendium of Neutron Spectra.[3] These spectra and associated DR were expected to be similar but not an exact match for the spectra in each experiment. The simulated spectrum for GODIVA was obtained from the results of a dosimetry exercise, of which the PNS was a part.[25]

The first experimental DR that was unfolded was for a reference calibration ^{252}Cf source at LLNL. The PNS was placed 3 m from the source with the positive X-axis pointed toward the source. The PNS was exposed for 4650.9 s with a dose rate of 79.98 mR/h. A total dose of 103.4 mR was recorded. The DR is shown in Fig. 3a. In a similar fashion, the PNS was exposed to a reference AmBe source at LLNL, and the DR is shown in Fig. 3b.

The GODIVA-IV reactor, referred to as GODIVA, is an assembly comprising approximately 65 kg of uranium.[20] It is a fast burst reactor, which means it is an unmoderated, unreflected bare core. The neutrons released from uranium fission have a mean energy per neutron of about 2 MeV. The PNS was exposed to a single prompt burst of GODIVA. The measured neutrons include those directly from the assembly and from room-returned scattered neutrons in the facility. The total neutron yield of the GODIVA pulse is unknown. This experiment represents a metal criticality safety accident that the PNS was designed to measure.

The NIF is a fusion research facility with the goal to induce fusion with high energy gain. The facility uses lasers to heat a target containing deuterium (D) and tritium (T) to over 3 million ℃. This causes fusion between two D atoms and fusion between D and T atoms. The former, D-D fusion, releases neutrons with energy of 2.45 MeV, and the latter, D-T fusion, releases neutrons with energy of 14.1 MeV. Exposing the PNS in this way represents a nuclear accident at an accelerator-based facility.

V. UNFOLDING NEUTRON SPECTRA

Many unfolding algorithms, such as those mentioned in Sec. I, require an input a priori spectrum. The accuracy of the output spectrum is heavily dependent on the accuracy of the a priori spectrum. For well-characterized sources, such as ^{252}Cf and AmBe, an accurate a priori spectrum can be obtained from literature, but because of differences in experimental setups, it will have various degrees of inaccuracies. To avoid inaccuracies present in other unfolding algorithms, an algorithm developed at LLNL was used to unfold the spectra from the experimental DRs. This algorithm is presented in more detail in a companion paper written by Maggi. In short, this algorithm avoids the use of an a priori spectrum and features two iteration loops: a larger outer loop and a smaller inner loop that is nested within the outer loop. For each outer loop, a starting spectrum is calculated by multiplying the pseudo-inverse of the DRM with the DR. Within the inner loop, the calculated spectrum is modified slightly and then used to calculate a DR using Eq. (1). The accuracy is calculated using Eq. (4):

$$\varepsilon_j = \sqrt{\sum \left(N_{k,exp} - N_{k,calc}\right)^2} \quad , \tag{4}$$

where k = inner loop iteration number; j = index of the detector; subscripts *exp* and *calc* = experimental and calculated DRs, respectively. If the spectrum modifications lead to a more accurate DR ($\varepsilon_{k+1} lt; \varepsilon_k$), then the modifications are kept for the next iteration. After all inner loops are completed, the outer loop completes with a final accuracy check and saves the final output spectrum. The next outer loop starts with a new calculated starting spectrum.

For each outer loop, the unfolded spectrum is saved into a variable. At the end of the algorithm, there are a number of spectra equal to the number of outer loop iterations. The median and standard deviation of the spectrum at each energy bin is calculated. Finally, an unfolded DR is calculated using the median spectrum.

VI. UNFOLDING STRATEGY

As mentioned in Sec. III.B, two separate DRMs were obtained for the PNS. The development of two separate DRMs is due to dependence of the DR on the position of the neutron source. The planar source DRM, referred to as DRM(p), approximates the direct neutron beam from an experimental source. The spherical source DRM, referred to as DRM(s), approximates the response function for backscattered neutrons from environmental factors. When the spectrum was unfolded with DRM(p), only neutrons in the high-energy region were unfolded, and when the spectrum was unfolded with DRM(s), only neutrons in the low-energy region were unfolded (see Figs. 4 and 5). For this research, both were used in coordination to more accurately unfold the spectrum.

Because of the placement of the neutron sources in the simulation, each DRM has a bias for the desired use case. An example of this bias is shown in Fig. 4. DRM(p) was used with the full DR to unfold a spectrum, and upon inspection, the unfolded DR more closely matches the

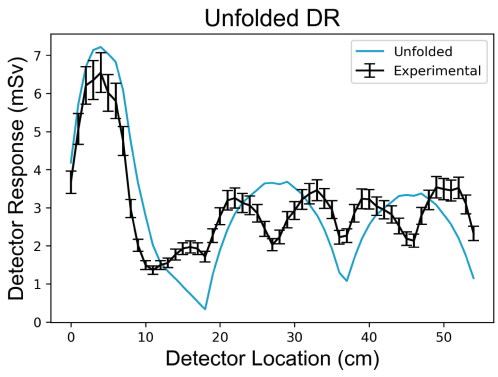

(a) DRM(d) unfolded DR

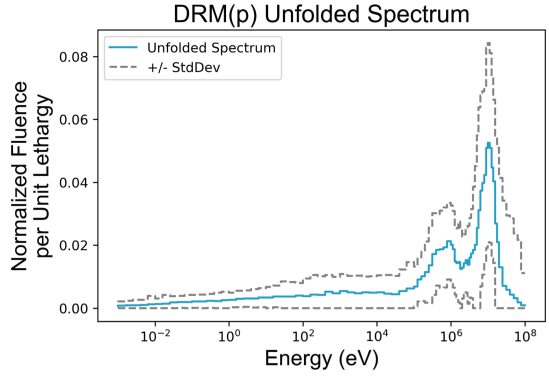

(b) DRM(d) unfolded spectrum

Fig. 4. Results of unfolding using only DRM(d).

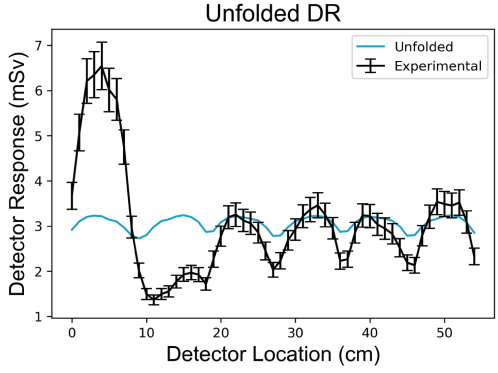

(a) DRM(i) unfolded DR

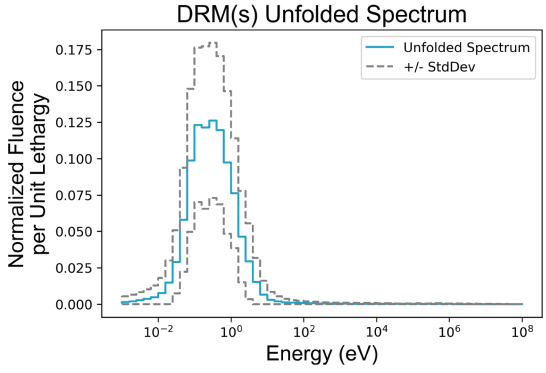

(b) DRM(i) unfolded spectrum

Fig. 5. Results of unfolding using only DRM(i).

positive *X*-axis detectors, but much less so for the axes. Similarly, when DRM(s) was used with the full DR, shown in Fig. 5, the unfolded DR more closely matches the DRs of the *Y*-axis and *Z*-axis. The inaccuracies in each unfolding stems from the physical nature of neutrons. In the experiment, a significant number of neutrons travel straight from the source to the PNS, and a significant number of neutrons are backscattered from the environment to the PNS. To minimize the bias of each DRM, the experimental DR was split into the direct response (using only the 10 positive *X*-axis DRs) and the indirect response (using the remaining 45 DRs).

In Fig. 4, the unfolded DR matches the experimental response for the positive *X*-axis values but becomes less accurate for the remaining DRs. This is due to room-scattered neutrons interacting with the PNS. For the results shown in Sec. VII, the direct response was unfolded using the algorithm described in Sec. V. This resulted in a spectrum with a bias for high-energy neutrons. By assuming that this spectrum is an accurate partial representation of the full spectrum, it was used to calculate the full DR using Eq. (1). This direct-calculated DR then represents only part of the experimental DR. By subtracting the direct DR from the experimental DR, an indirect DR remains, which corresponds to the effects of the backscattered neutrons on the PNS. Using the indirect DR and the DRM(s) as the starting point in the unfolding algorithm, the remaining portion of the spectrum can be unfolded.

If the direct and indirect spectra are assumed to represent a portion of the true spectrum, then there exists a weighted sum of the two that represents the full spectrum. To attain this weighted sum, a simple iterative approach was used to search all possible weights of DRs calculated through the unfolded spectra to find the best weighted sum match. This iterative approach was performed in 1% increments for both DRs. For example, 1% of the direct unfolded DR was summed with 1% of the indirect unfolded DR, and the sum of the difference of the squares between the weighted sum DR and experimental DR was calculated.

Then, 1% of the direct DR was summed with 2% of the indirect DR, and so on until all weighted sums were compared to the experimental DR. This led to the final reported value for each of the experimental DRs reported in Sec. VII. The corresponding weighted sum spectrum was then used with the ANSI dose conversion units to determine the expected dose someone would receive at that location.[5]

VII. RESULTS

The unfolding results for each of the four experimental DRs are shown in this section. For each experimental DR, there are three figures each with two subfigures. The first figure shows the results of the direct unfolding in which only the positive X-axis detectors were used. In the left figure, a comparison is made of the unfolded DR (blue) and experimental DR (black). The error bars for the unfolded DR correlate to the propagated errors of the standard deviations for each energy bin in the unfolded energy spectrum. The error bars for the experimental DR are as described in Sec. IV. In the right figure, a comparison is made of the unfolded energy spectrum (blue) and an energy spectrum from a similar source, if available (black). An exact match between these two is not expected because the measured spectrum from any particular source will vary depending on environmental factors present during the exposure to that source. However, various features of the energy spectrum should be common between the two. These features include the location of the maximum of the energy peaks that are present and the full-width at half-maximum (FWHM) of each spectrum. The ^{252}Cf and AmBe sources were both calibration sources, and the expected dose was calculated and can be compared to the dose calculated after unfolding. The data from GODIVA were analyzed by various organizations, and the doses were reported and can be compared.[25]

The quality of each unfolding can be calculated using the following metrics: dose comparison, unfolded DR error, and location and FWHM of the energy peaks. The dose comparison directly relates to the main purpose of this work: to calculate neutron dose to within 30% of the expected dose. This is the main metric to which the accuracy of the unfolded spectrum will be compared. As an additional measure of comparison, the average error of the unfolded DR to the experimental DR will be given. Finally, the location and FWHM of each energy peak will be given.

VII.A. CALIFORNIUM-252 UNFOLDED SPECTRUM

The results of unfolding the ^{252}Cf DR are shown in Figs. 6, 7, and 8. These results are summarized in Table I. The ^{252}Cf source is a calibration source used at LLNL, and the dose was calculated for the exposure time to be 103.4 mR. As expected, neither the direct nor indirect unfolded spectra matched all features of the expected spectrum, while the weighted sum results matched the features and most importantly calculated the dose to 8.07%.

VII.B. AmBe Unfolded Spectrum

The results of unfolding the AmBe DR are shown in Figs. 9, 10, and 11. These results are summarized in Table II. The dose expected from this AmBe source is unknown, so the features shown in the unfolding are the only metrics by which to measure. In Fig. 9, it appears that the direct spectrum unfolding captures all of the characteristics in the reference spectrum. In Table II, the direct unfolded DR has the lowest error on average

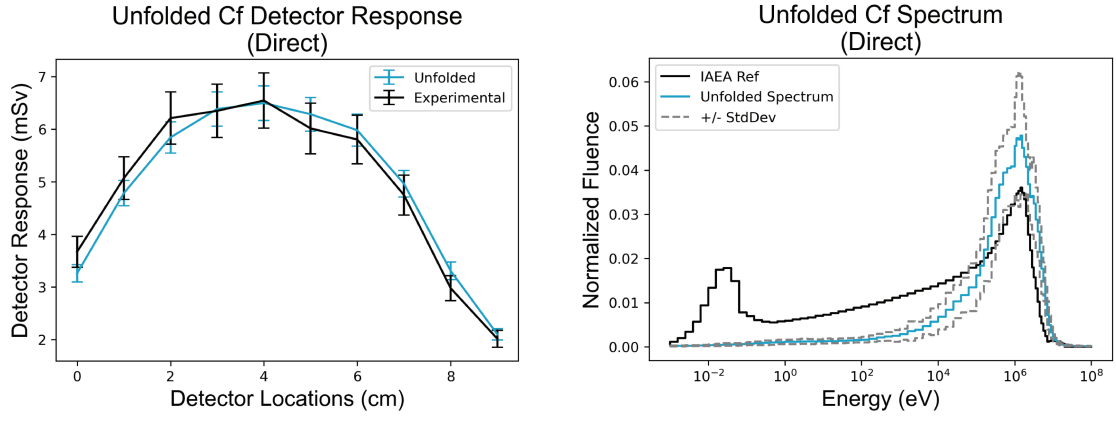

(a) Direct unfolded DR

(b) Direct unfolded spectrum

Fig. 6. The unfolded DR and neutron spectrum using the direct DRM for ^{252}Cf.

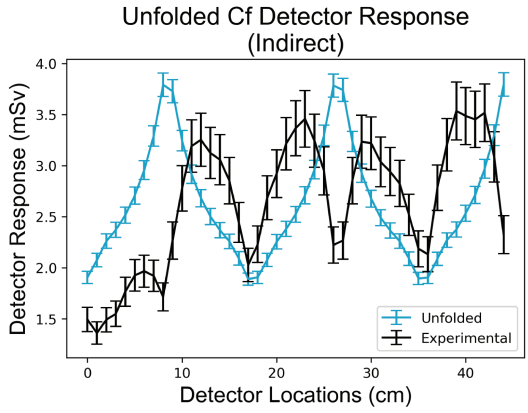

(a) Indirect unfolded DR

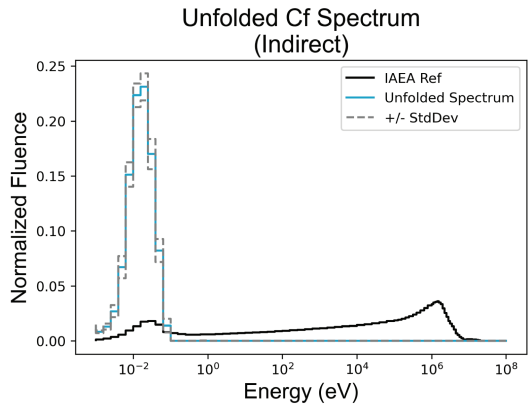

(b) Indirect unfolded spectrum.

Fig. 7. The unfolded DRs and neutron spectrum using the indirect DRM for ^{252}Cf.

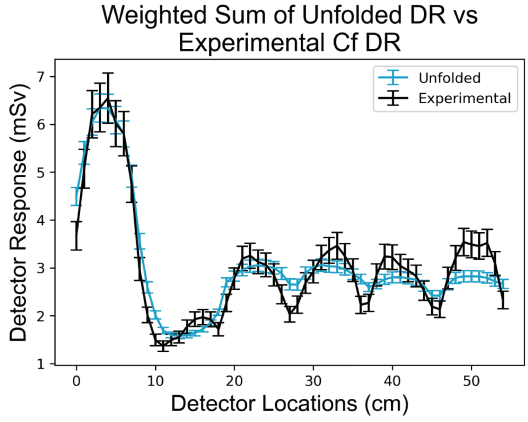

(a) Weighted sum unfolded DR

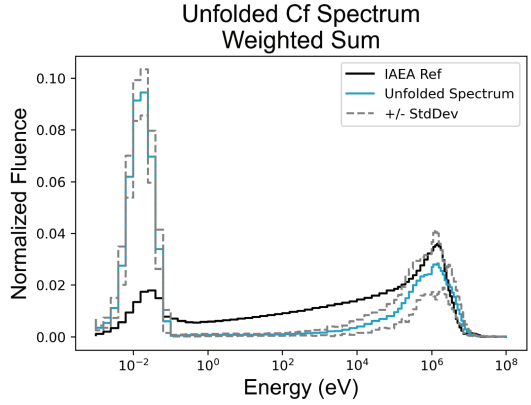

(b) Weighted sum unfolded spectrum

Fig. 8. The weighted sum of the unfolded DRs and the spectrum for the ^{252}Cf source.

TABLE I

Summary of the Results for Unfolding the ^{252}Cf DR

Unfolding Method	Dose (mRad)	Dose Percent Error	Detector Response Average Error (%)	Low Energy (meV)		High Energy (MeV)	
				Peak	FWHM	Peak	FWHM
Direct	118.85 ± 4.81	14.94	3.36	—	—	1.00–1.26	1.10
Indirect	1.14 ± 0.03	98.90	53.70	15.80–39.80	21.1	—	—
Weighted sum	95.05 ± 4.81	8.07	11.03	15.80–39.80	21.1	1.00–1.26	1.10

compared to the other unfolding steps. This is supported by Figs. 10 and11, where the weighted sum results do not drastically vary from the direct results. In other words, the indirect unfolded results were given very little weight in calculating the weighted sum. This could be due to the amount of neutrons scattered back to the PNS being negligible.

VII.C. GODIVA Unfolded Spectrum

The results of unfolding the GODIVA DR are shown in Figs. 12, 13, and 14. These results are summarized in Table III. This DR was obtained during an exercise, and the expected dose has been independently calculated and reported to be 0.86 Gy.[25] The spectrum was also unfolded

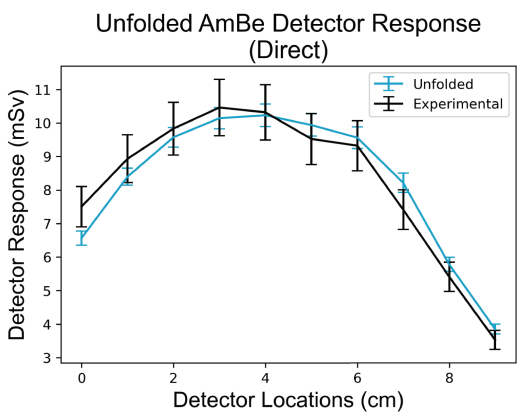

(a) Direct unfolded DR

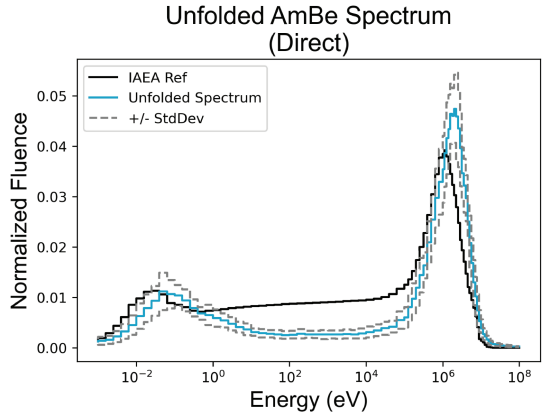

(b) Direct unfolded spectrum

Fig. 9. The unfolded DR and neutron spectrum using the direct DRM for AmBe.

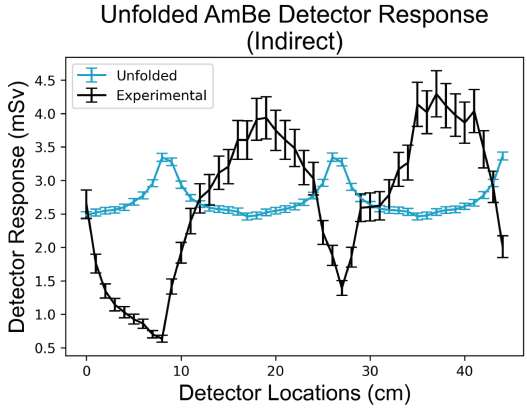

(a) Indirect unfolded DR

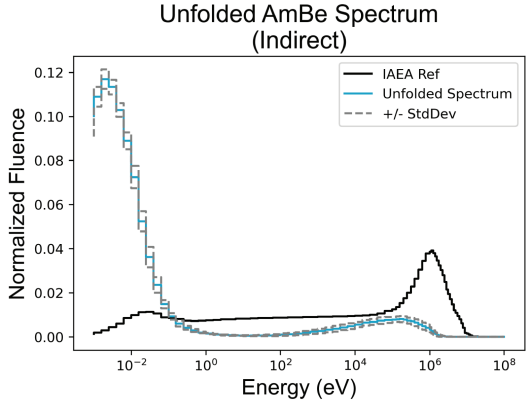

(b) Indirect unfolded spectrum.

Fig. 10. The unfolded DRs and neutron spectrum using the indirect DRM for AmBe.

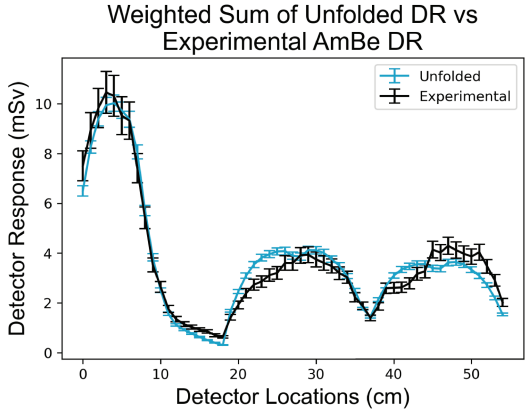

(a) Weighted sum unfolded DR

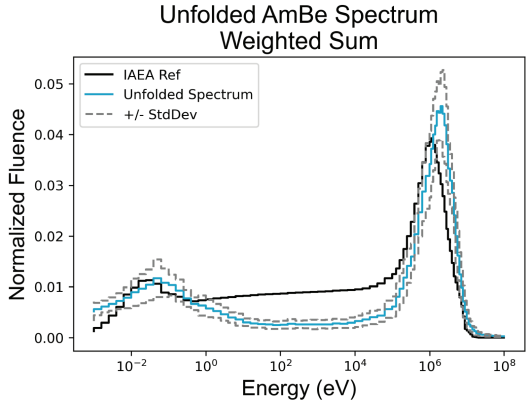

(b) Weighted sum unfolded spectrum

Fig. 11. The weighted sum of the unfolded DRs and the spectrum for the AmBe source.

TABLE II

Summary of the Results for Unfolding the AmBe DR

Unfolding Method	Dose (mRad)	Dose Percent Error	Detector Response Average Error (%)	Low Energy (meV)		High Energy (MeV)	
				Peak	FWHM	Peak	FWHM
Direct	201.0 ± 7.10	—	4.01	158.0 to 398.0	1.00 (MeV)	2.00 to 2.51	1.45
Indirect	0.48 ± 0.07	—	88.57	1.58 to 3.98	18.8	—	—
Weighted Sum	225.6 ± 7.07	—	14.84	158.0 to 398.0	1.00 (MeV)	2.00 to 2.51	1.61

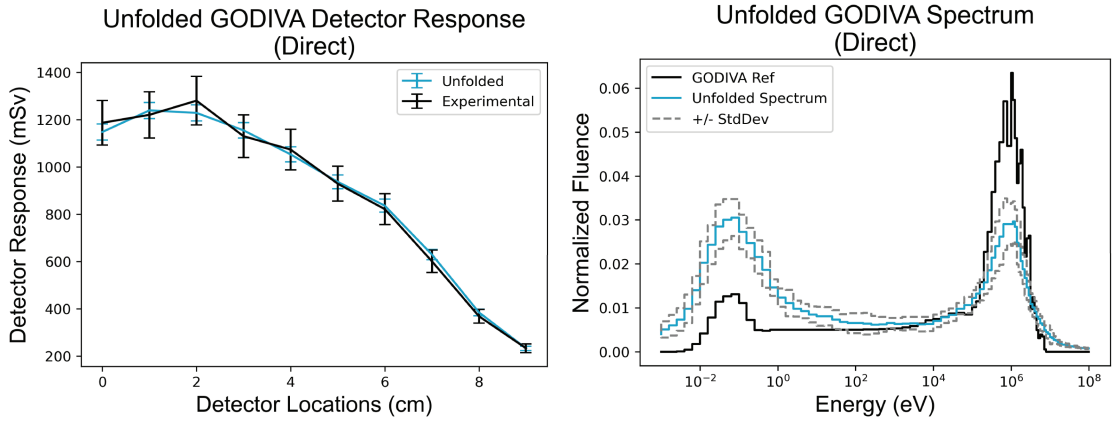

(a) Direct unfolded DR (b) Direct unfolded spectrum

Fig. 12. The unfolded DRs and neutron spectrum using the direct DRM for the GODIVA neutron field.

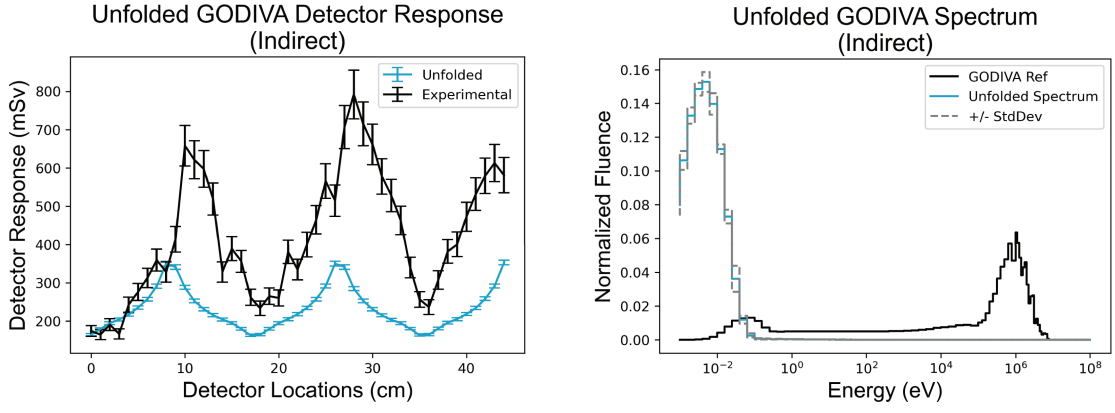

(a) Indirect unfolded DR (b) Indirect unfolded spectrum

Fig. 13. The unfolded DRs and neutron spectrum using the indirect DRM for the GODIVA neutron field.

following the exercise and can be used as the reference spectrum to compare to. The results of the direct spectrum unfolding are shown in Fig. 12b. Although the magnitude is different, the locations of both the high-energy peak and the low-energy peak match the peaks in the reported spectrum. However, for the indirect and weighted sum unfolded spectra, the low-energy region of the spectrum becomes overrepresented. This is overrepresentation likely means that

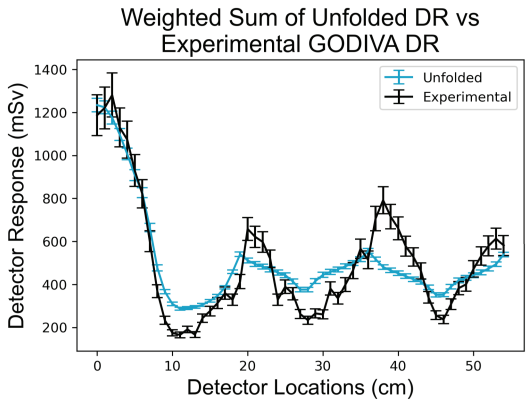

(a) Weighted sum unfolded DR

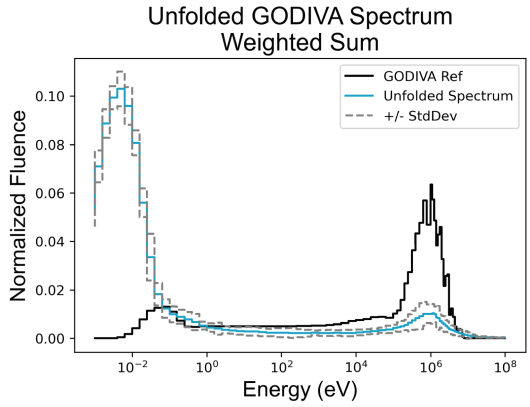

(b) Weighted sum unfolded spectrum

Fig. 14. The weighted sum unfolded DRs and spectrum.

TABLE III

Summary of the Results for Unfolding the GODIVA DR

Unfolding Method	Dose (Gy)	Dose Percent Error	Detector Response Average Error (%)	Low Energy (meV)		High Energy (MeV)	
				Peak	FWHM	Peak	FWHM
Direct	0.15 ± 0.01	83.12	2.50	63.1 to 158.0	90.0	1.12–1.41	1.06
Indirect	0.00 ± 0.00	99.72	40.15	3.98 to 10.0	3.69	—	—
Weighted sum	0.11 ± 0.01	86.73	25.57	3.98 to 10.0	9.49	1.12–1.41	1.06

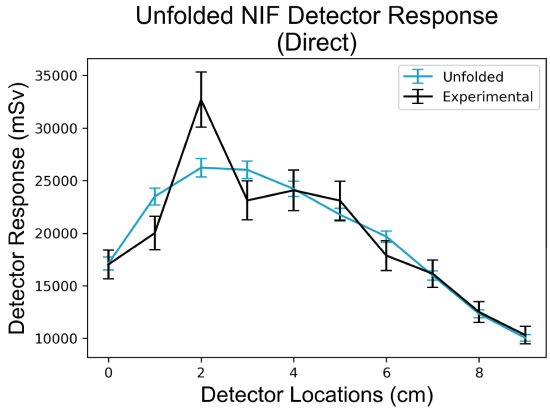

(a) Direct unfolded DR

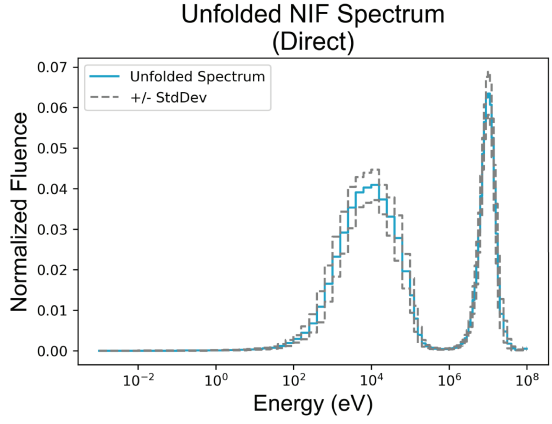

(b) Direct unfolded spectrum

Fig. 15. The unfolded DR and neutron spectrum using the direct DRM for a NIF shot.

the PNS was not subjected to very many room-scattered neutrons and the direct unfolding alone is best for the fit. Additional work will need to be done to determine the cause of the mismatch in magnitudes of the peaks in the direct unfolded spectrum.[26]

VII.D. NIF Unfolded Spectrum

The results of unfolding the NIF DR are shown in Figs. 15, 16, and17. These results are summarized in Table IV. In this case, there is no spectrum that can be used for

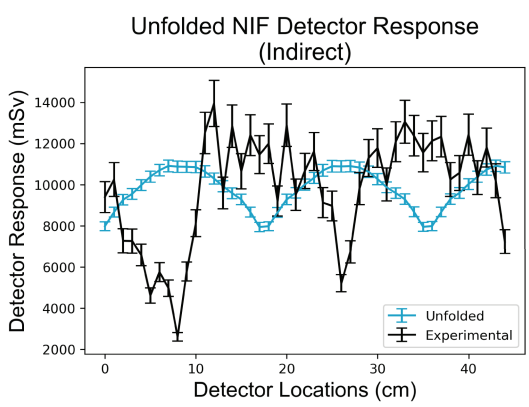

(a) Indirect unfolded DR

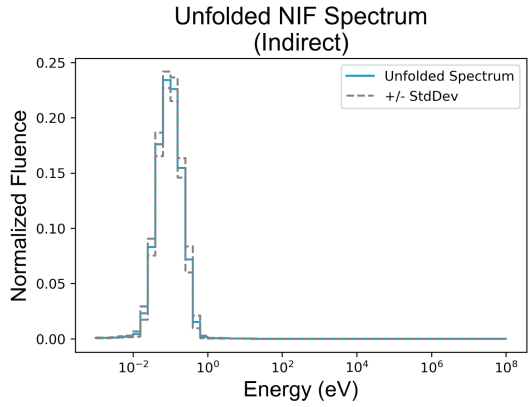

(b) Indirect unfolded spectrum

Fig. 16. The unfolded DRs and neutron spectrum using the indirect DRM for a NIF shot.

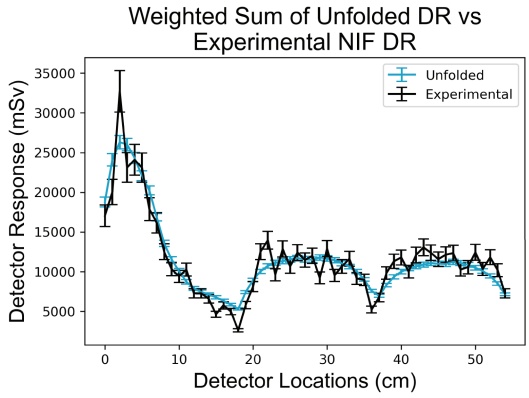

(a) Weighted sum unfolded DR

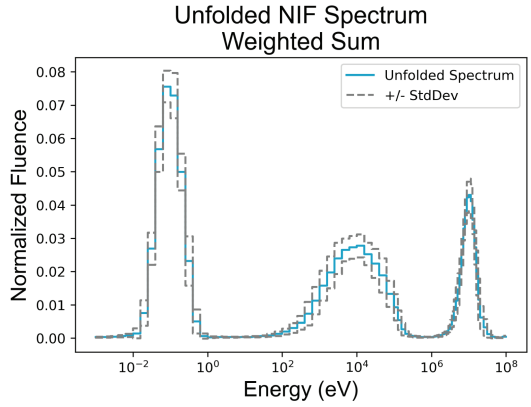

(b) Weighted sum unfolded spectrum

Fig. 17. The weighted sum unfolded DRs and spectrum.

direct comparison. Notably, the direct unfolded spectrum contains two peaks, although they are at slightly different energies than would be expected of a T-T fusion event (releases neutrons at 14.1 MeV) and a D-T fusion event (releases neutrons at 2.45 MeV). This is likely due to the position of the PNS during the experiment and the interactions of neutrons with the environment on the way to the detectors within the PNS.

VIII. CONCLUSION

In this work, four different experimental DRs were unfolded. The main goal of this work was to introduce the PNS as a detection system that provides the information needed to accurately unfold neutron energy spectra. An unfolding algorithm developed by Maggi at LLNL was used to unfold, and furthermore, an unfolding strategy was developed to mitigate the lack of real-world information present in the simulated DRM. The metrics used for determining the effectiveness of unfolding were dose comparison (if available), comparison of the energy peaks in the spectrum, and average error of the calculated DR compared to the experimental DR. Although there is room for improvement, the PNS was able to provide the information needed to unfold a neutron energy spectrum from each DR.

The first unfolded spectrum was from the DR obtained in the presence of a ^{252}Cf calibration source, which allowed for a direct comparison of the calculated dose. When comparing the dose, the best results were obtained after performing the weighted sum unfolding method, and the associated error was 8.07%. However, the best fit for the DR was obtained from direct unfolding.

The second unfolded spectrum was from the DR obtained in the presence of an AmBe source. The

TABLE IV
Summary of the Results for Unfolding the NIF DR

Unfolding Method	Dose (Gy)	Dose Percent Error	Detector Response Average Error (%)	Low Energy (meV)		High Energy (MeV)	
				Peak	FWHM	Peak	FWHM
Direct	4.63 ± 0.22	—	7.83	—	—	5.62 to 7.08	1.16
Indirect	0.03 ± 0.00	—	62.65	100.0 to 251.0	118	—	—
Weighted sum	3.22 ± 0.19	—	13.58	100.0 to 251.0	118	5.62 to 7.08	1.16

expected dose from this source was unknown, so the metrics for determining the accuracy of this unfolded spectrum were the error in the DR and the features of the spectrum. The results of this unfolding show that the direct unfolded spectrum was the most accurate with an average error of the DR at 4.01%. Additionally, the unfolded spectrum contained all of the features of the reference spectrum.

The third unfolded spectrum was from the DR in the presence of the GODIVA reactor. The data recorded for this experiment were also processed as part of a larger exercise in which other organizations unfolded the data to obtain a neutron spectrum. Again, in this case, it seems that the direct unfolded response is the best fit for the data, and the error in the DR is only 2.50%. However, the calculated dose is much different from that reported from the exercise. This is due to the differences in the magnitudes of each peak in the energy spectrum. The dose conversion factors are one to two orders of magnitude higher for the high-energy peak compared to the low-energy peak.

The final unfolded spectrum was from the DR in the presence of the NIF's fusion source. These data have no direct spectrum or dose to which it can be compared. Notably, in this case, the direct unfolding resulted in a spectrum with two high-energy peaks, and the indirect unfolding resulted in a spectrum with one low-energy peak. The highest-energy peak correlates to the T-T fusion events, and the lowest-energy peak correlates to the D-T fusion events. The energies of these peaks are lower than would be expected for each of those events, but this is attributed to the loss of energies as neutrons travel from the source of the events to the PNS itself.

In summary, the PNS is well equipped to unfold neutron energy spectra. The multistep process to identify the differences between direct neutrons and indirect neutrons was able to provide more accurate information in some of the cases. More work will be needed to improve upon this. The next step in future studies will be to more accurately characterize the PNS through simulations and rigorous experiments. Improvements and optimizations can be made on the unfolding algorithm itself as well as on the direct/indirect unfolding process. Finally, new methods of unfolding, such as feed-forward and convolutional neural networks, will be used to determine if more accurate results can be obtained.

Acknowledgments

The work performed during this research could not have been done without the guidance and mentorship from Richard

Vasques. Additionally, the support from Daniel Siefman and Paul Maggi was instrumental throughout. Additionally, Paige Witter provided much of the groundwork and additional help in attaining these results.

The views expressed in this article are those of the authors and do not reflect the official policy or position of the U.S. Air Force, U.S. Department of Defense, or U.S. Government.

Disclosure Statement

No potential conflict of interest was reported by the author(s).

References

1. DOE-STD-1098-2017, *Radiological Control*, U.S. Department of Energy (2017).
2. *Preparedness and Response for a Nuclear or Radiological Emergency*, IAEA Safety Standards Series No. GSR Part 7, General Safety Requirements, International Atomic Agency, Vienna (2015).
3. R. V. GRIFFITH et al., "Compendium of Neutron Spectra and Detector Responses for Radiation Protection Purposes," International Atomic Energy Agency (1990).
4. ANSI/ANS-6.1.1-1991, *Neutron and Gamma-Ray Fluence-to-Dose Factors*, American Nuclear Society, Westmont, Illinois (1991).
5. ANSI/HPS N13.3-2013, *Dosimetry for Criticality Accidents*, Health Physics Society (2013).
6. M. REGINATTO, "Overview of Spectral Unfolding Techniques and Uncertainty Estimation," *Radiat. Meas.*, **45**, *10*, 1323 (2010); http://dx.doi.org/10.1016/j.radmeas.2010.06.016.
7. J. B. BIRKS, *The Theory and Practice of Scintillation Counting: International Series of Monographs in Electronics and Instrumentation*, Vol. 27, Elsevier (2013).
8. A. GUEORGUIEV et al., "Composite Neutron Gamma Detector," *Proc. 2015 IEEE Nuclear Science Symp. and Medical Imaging Conf. (NSS/MIC)*, San Diego, California, October 31–November 7, 2015, p. 1056, Institute of Electrical and Electronics Engineers (2015).
9. A. FOSTER et al., "On the Fabrication and Characterization of Heterogeneous Composite Neutron Detectors with Triple-Pulse-Shape-Discrimination Capability," *Nucl. Instrum. Methods Phys. Res. Sec. A*, **954**, 161681 (2020); http://dx.doi.org/10.1016/j.nima.2018.11.140.
10. N. ZAITSEVA et al., "Pulse Shape Discrimination with Lithium-Containing Organic Scintillators," *Nucl. Instrum. Methods Phys. Res. Sec. A*, **729**, 747 (2013); http://dx.doi.org/10.1016/j.nima.2013.08.048.
11. R. L. BRAMBLETT et al., "A New Type of Neutron Spectrometer," *Nucl. Instrum. Methods*, **9**, *1*, 1 (1960); http://dx.doi.org/10.1016/0029-554x(60)90043-4.
12. W. MCELROY et al., "A Computer-Automated Iterative Method for Neutron Flux Spectra Determination by Foil Activation. Volume 1. A Study of the Iterative Method," Atomics International (1967).
13. M. REGINATTO and P. GOLDHAGEN, "MAXED, A Computer Code for the Deconvolution of Multisphere Neutron Spectrometer Data Using the Maximum Entropy Method," U.S. Department of Energy (1998).
14. D. V. JORDAN et al., "Methods and Instruments for Fast Neutron Detection," Pacific Northwest National Laboratory (2005).
15. K. WEISE and M. MATZKE, "A Priori Distributions from the Principle of Maximum Entropy for the Monte Carlo Unfolding of Particle Energy Spectra," *Nucl. Instrum. Methods Phys. Res. Sec. A*, **280**, *1*, 103 (1989); http://dx.doi.org/10.1016/0168-9002(89)91277-1.
16. G. CHOUDALAKIS, "Fully Bayesian Unfolding," arXiv preprint arXiv:1201.4612 (2012); https://doi.org/10.48550/arXiv.1201.4612.
17. S. A. HOSSEINI, "Neutron Spectrum Unfolding Using Artificial Neural Network and Modified Least Square Method," *Radiat. Phys. Chem.*, **126**, 75 (2016); 10.1016/j.radphyschem.2016.05.010.
18. M. BOUHADIDA et al., "Neutron Spectrum Unfolding Using Two Architectures of Convolutional Neural Networks," *Nucl. Eng. Technol.*, **55**, *6*, 2276 (2023); http://dx.doi.org/10.1016/j.net.2023.03.025.
19. C. CAO et al., "An Adaptive Deviation-Resistant Neutron Spectrum Unfolding Method Based on Transfer Learning," *Nucl. Eng. Technol.*, **52**, *11*, 2452 (2020); http://dx.doi.org/10.1016/j.net.2020.04.028.
20. J. GÓMEZ-ROS et al., "A Multi-Detector Neutron Spectrometer with Nearly Isotropic Response for Environmental and Workplace Monitoring," *Nucl. Instrum. Methods Phys. Res. Sect. A*, **613**, *1*, 127 (2010); http://dx.doi.org/10.1016/j.nima.2009.11.011.
21. J. A. KULESZA et al., "MCNP® Code Version 6.3.0 Theory & User Manual," LA-UR-22-30006, Rev. 1, Los Alamos National Laboratory (2022); http://dx.doi.org/10.2172/1889957;https://www.osti.gov/biblio/1889957.
22. D. BROWN et al., "ENDF/B-VIII.0: The 8th Major Release of the Nuclear Reaction Data Library with CIELO-Project Cross Sections, New Standards and Thermal Scattering Data," *Nucl. Data Sheets*, **148**, 1 (2018); http://dx.doi.org/10.1016/j.nds.2018.02.001;ttps://www.sciencedirect.com/science/article/pii/S0090375218300206.
23. T. P. MCLAUGHLIN et al., "A Review of Criticality Accidents 2000 Revision," Los Alamos National Laboratory (2000).

24. N. PETOUSSI-HENSS, "Conversion Coefficients for Radiological Protection Quantities for External Radiation Exposures," ICRP Publication 116, *Ann. ICRP*, **40**, *2–5*, 1 (2010); http://dx.doi.org/10.1016/j.icrp.2011.10.001.

25. A. S. TAMASHIRO et al., "IER-538 CED4A Report: Godiva-IV Dosimetry Exercise 2022," Lawrence Livermore National Laboratory (2023); http://dx.doi.org/10.2172/1964010; https://www.osti.gov/biblio/1964010.

26. J. GODA et al., "A New Era of Nuclear Criticality Experiments: The First 10 Years of Godiva IV Operations at NCERC," *Nucl. Sci. Eng.*, **195**, *Suppl. 1*, S55 (2021); http://dx.doi.org/10.1080/00295639.2021.1947103.